Journal of Materials Chemistry A

Accepted Manuscript

ROYAL SOCIETY OF CHEMISTRY

www.rsc.org/materialsA

Journal Name

ARTICLE

Multilayered Paper-Like Electrodes Composed of Alternating Stacked Mesoporous Mo_2N Nanobelts and Reduced Graphene Oxide for Flexible All-Solid-State Supercapacitors

Received 00th January 20xx,
Accepted 00th January 20xx

DOI: 10.1039/x0xx00000x

www.rsc.org/

Guoqiang Ma,[a] Zhe Wang,[a] Biao Gao,[b] Tianpeng Ding,[a] Qize Zhong,[a] Xiang Peng,[c] Jun Su,[a] Bin Hu,[a] Longyan Yuan,[a] Paul K Chu,[c] Jun Zhou[a] and Kaifu Huo*[a]

Flexible all-solid-state supercapacitors (SCs) have great potential in flexible and wearable electronics due to the safety, flexibility, high power density, and portability. The energy storage properties of SCs are determined mainly by the composition, conductivity as well as the configuration of the integrated electrode material. Herein, a freestanding multilayered film electrode consisting of alternating stacked mesoporous Mo_2N nanobelts and rGO nanosheets (MMNNBs/rGO) is described. It has a high mass loading of 95.6 wt% of Mo_2N active materials and boasts high areal capacitances of 142 and 98 mF cm^{-2} at current densities of 1 and 150 mA cm^{-2}. All-solid-state SCs fabricated by sandwiching two thin and flexible freestanding MMNNBs/rGO hybrid electrodes with the poly (vinyl alcohol) (PVA) /H_3PO_4/silicotungstic acid (SiWA) gel electrolyte show a high volumetric capacitance of 15.4 F cm^{-3} as well as energy and power densities of 1.05 mWh cm^{-3} and 0.035 W cm^{-3} at a current density of 0.1 A cm^{-3} based on the volume of whole cell. After 4000 charging-discharging cycles, the flexible SC retains 85.7% initial capacitance thus exhibiting good cycling stability. This work provides a versatile method for flexible and high-performance ceramic-based nanohybrid films for SCs, and has immense potential in flexible and wearable electronics.

Introduction

As portable and flexible electronics become increasingly popular, there is a growing demand for flexible energy storage devices.[1-4] In this respect, flexible all-solid-state supercapacitors (SCs) provide potentially safe, flexible, lightweight, portable, and environmentally friendly power sources that can be integrated with flexible and wearable electronic devices to "power up" them.[5-7] Although flexible SCs share many similar components and working principles as conventional SCs, they require flexible electrodes with good capacitive properties, coupled with shape-conformable solid-state electrolytes, and/or soft packaging materials.[8, 9] Thus, power and energy supply as well as cyclic stability of flexible SCs are not compromised by bending, folding, or other deformation modes.

SCs are mainly classified into electric double layer capacitors (EDLCs) and pseudocapacitors according to charge storage mechanism.[10, 11] The EDLCs store charges by ion absorption/desorption at the interface between the electrolyte and large surface area electrodes such as carbon nanotubes, activated carbon nanofibers, and graphene.[12, 13] Although carbon-based flexible SCs have been demonstrated to have a high power density, fast charging and discharging rates, and long cycle lifetime, they generally suffer from a small energy density due to the low specific capacitance of carbon-based electrodes.[10, 14, 15] Contrary to EDLCs, pseudocapacitors store charges by the fast and reversible redox reactions at or near the surface of the pseudocapacitive electrode materials.[16] Pseudocapacitive materials such as transition metal oxides (e.g. MnO_2,[17, 18] Co_3O_4,[19] VO,[20], and NiO[21]) and conducting polymers (e.g. polyaniline,[22] polypyrrole[23]) can produce substantially higher specific capacitances (300-2000 F/g) than carbon materials. Therefore, pseudocapacitors generally deliver a bigger energy density than EDLCs. However, the low electrical conductivity of metal oxides and instability intrinsically associated with conductive polymers generally lead to poor rate capability, low power density, and/or poor cycling stability.[24-27]

Some metal nitrides such as molybdenum nitrides (MoN, Mo_2N, Mo_3N_2) and vanadium nitride (VN) have good electrical conductivity like metals and large specific capacitances comparable to those of many metal oxides.[28-32] Therefore, they are promising electrode materials for high-performance SCs. Moreover, these metal nitrides generally have large volumetric energy densities due to the big tap density. In practical applications involving flexible and portable devices, the volumetric energy density of SCs is generally more important than gravimetric energy density because of the limited packing space.[33, 34] MoN and Mo_2N were firstly reported as SC electrode materials in 1998.[35] Recently, Li *et al*. showed that

[a] *Wuhan National Laboratory for Optoelectronics, School of Optical and Electronic Information, Huazhong University of Science and Technology, Wuhan 430074, China.*
[b] *The State Key Laboratory of Refractories and Metallurgy, Wuhan University of Science and Technology, Wuhan 430081, China.*
[c] *Department of Physics and Materials Science, City University of Hong Kong, Tat Chee Avenue, Kowloon, Hong Kong, China.*
†Electronic Supplementary Information (ESI) available: See DOI: 10.1039/x0xx00000x

Mo_2N nanoparticles had a high specific capacitance of 172 F/g in a 1 mol/L H_2SO_4 electrolyte[36] and Lee et al. demonstrated that mesoporous Mo_3N_2 nanowires exhibited a capacity of over 200 F g^{-1} even at a large charging/discharging rate of 200 mV s^{-1}.[Ref. 37] However, although molybdenum nitrides possess excellent capacitive properties, all-solid-state flexible SCs based on molybdenum nitrides have rarely been reported.

Herein, a simple method to fabricate flexible mulitilayered film electrodes consisting of alternating stacked mesoporous Mo_2N nanobelts (NBs) and reduced graphene oxide nanosheets (MMNNBs/rGO) is described. The free-standing MMNNBs/rGO film electrodes have several advantages as flexible electrodes for high-performance flexible SCs. First of all, the mesoporous Mo_2N NBs provide a large surface area and more active sites accessible for charge storage, leading to high utilization efficiency and high specific capacitance of the Mo_2N active materials. Secondly, the rGO layers between the Mo_2N NBs layers provide the robust mechanical infrastructure compatible with the intrinsic rigidity of Mo_2N, resulting in robust flexibility and mechanical integrity of the MMNNBs/rGO mulitilayered film. Thirdly, the stacked multilayered structure significantly improves the mass loading of Mo_2N active materials (as high as 95.6 wt. %) while retaining the good mechanical integrity and flexibility of MMNNBs/rGO without needing foreign binding agents. Fourthly, the alternating stacked and interconnected networks of MMNNBs/rGO provide high conductivity and short diffusion length for electrons and ions resulting in large capacitance and high rate capability. As a consequence, the free-standing MMNNBs/rGO multilayered film electrode can deliver large areal capacitances of 142 and 98 mF cm^{-2} at current densities of 1 and 150 mA cm^{-2}, respectively, and exhibits excellent cycling stability in an aqueous H_2SO_4 electrolyte with 93 % of the initial capacitance retained after 10,000 cycles. The all-solid-state flexible SCs fabricated by sandwiching two free-standing MMNNBs/rGO multilayered film electrodes with the poly (vinyl alcohol) (PVA) /H_3PO_4/silicotungstic acid (SiWA) (SiWA–H_3PO_4–PVA) gel electrolyte show a large volumetric capacitance of 15.4 F cm^{-3} at a current density of 0.1 A cm^{-3} and high energy density of 1.05 mW h cm^{-3} at power density of 0.035 W cm^{-3}. These values are much larger than most of the previous results obtained from quasi and all-solid-state flexible SCs.[38-45] To demonstrate the commercial potential in wearable or portable devices, a set of the SCs is integrated to power an liquid crystal display (LCD).

Experimental details

Preparation of MoO_3 nanobelts

All the chemical reagents were analytical grade and used as received without further purification. A hydrothermal method was implemented to synthesize MoO_3 NBs. Typically, 1.2 g molybdenum (Mo) powders (Aladdin, 99.5%) were added to 10 ml of H_2O_2 (30%) under vigorous stirring in an ice-water bath until the solution became transparent. The saffron yellow solution was diluted with 110 ml deionized water (DIW). After stirring for 30 min, the solution was transferred into a Teflon-lined stainless steel autoclave (60 ml) and heated to 180 °C for 3 days. The products were filtered and rinsed with DIW and alcohol thoroughly, followed by vacuum drying at 70 °C for 12 h.

Synthesis of MMNNBs and free-standing MMNNBs/rGO hybrid film

In a typical process, 32 mg of the MoO_3 NBs were dispersed in 35 ml of DIW containing 0.5 ml of the poly (diallyldimethylammonium chloride) (PDDA) solution under vigorous stirring to form positively charged MoO_3-PDDA by absorbing PDDA cations. The excess PDDA was removed by repetitive centrifugation/washing/re-dispersion. The GO powders purchased from Sixth Elements Hi-tech Development Co. Ltd. (Changzhou, China) were sonicated in 8 ml of DIW for 30 min by probe sonicater. The positively-charged MoO_3-PDDA was added dropwise to the GO suspension under ultrasonication. After further probe sonication for 5 min, the suspension was vacuum-filtered through a filter membrane (220 nm pore size) and washed by DIW for several times. After vacuum drying at 60 °C overnight, the free-standing MoO_3/GO hybrid film was peeled off from the filtration membrane, which was further thermally treated in a tube furnace in NH_3 at 750 °C for 30 min to produce free-standing MMNNBs/rGO hybrid film. The Mo_2N NBs were also fabricated under the same conditions by nitridation of MoO_3 NBs.

Assembly of flexible all-solid-state symmetric SCs

The all-solid-state flexible SCs were assembled by sandwiching two pieces of the MMNNBs/rGO hybrid paper electrodes with poly (vinyl alcohol) (PVA) /H_3PO_4/silicotungstic acid (SiWA) (SiWA–H_3PO_4–PVA) gel electrolyte and a separator (NKK, Nippon Kodoshi Corporation). The SiWA–H_3PO_4–PVA gel was prepared by mixing H_3PO_4 (6 g), SiWA (12 g), and PVA (6 g) in 60 ml of DIW and heated to 85 °C for 3 h under stirring. Prior to assembling, the two electrodes and separator were immersed in the SiWA–H_3PO_4–PVA electrolyte for about 10 min. The devices were solidified at room temperature for 12 h to remove excess water.

Characterization and electrochemical measurements

The morphology, structure, and composition of the samples were characterized by X-ray diffraction using Cu K_α radiation (λ = 1.5418 Å) (XRD, Philips X' Pert Pro), field-emission scanning electron microscopy (FE-SEM, FEI Nova 450 Nano), high-resolution transmission electron microscopy equipped with energy-dispersive X-ray spectroscopy (HR-TEM, FEI Titan G2 60-300), thermal analysis (STA449) and X-ray photoelectron spectroscopy (XPS, ESCALab250). The specific surface area was evaluated by N_2 adsorption (Micromeritics ACAP 2020 analyzer). The electrochemical performance was assessed by cyclic voltammetry (CV) and galvanostatic charging/discharging (GCD) measurements performed on an electrochemical workstation (CHI 660E). The electrochemical impedance was measured from 1 mHz to 1 MHz with a potential amplitude of 10 mV (Autolab PGSTAT302N). The cycle life was determined by a battery test system (MTI).

Results and discussion

The fabrication procedures of the flexible MMNNBs/rGO

multilayered paper electrodes and flexible all-solid-state SCs are illustrated in Scheme 1. Firstly, as-synthesized α-MoO_3 NBs were dispersed in PDDA solution by vigorous stirring to form positively-charged MoO_3-PDDA by absorbing PDDA cations. The positively-charged MoO_3-PDDA were then dispersed in a negatively-charged GO aqueous solution to form self-assembled MoO_3/GO nanocomposites due to electrostatic interaction. The free-standing MoO_3/GO hybrid films were acquired by vacuum filtering and peeled off from the filter membrane after drying at 60 °C overnight. They were further thermally treated at 750 °C under NH_3 for 30 min to produce free-standing MMNNBs/rGO hybrid films by reducing GO and nitriding MoO_3. The all-solid-state flexible SCs based on two symmetrical MMNNBs/rGO hybrid film electrodes were assembled using the SiWA-H_3PO_4-PVA gel electrolyte.

Fig. 1a depicts the SEM image of the hydrothermal product using Mo powder and H_2O_2 as precursors and shows the belt-like morphology with lengths up to tens of micrometers. The inset in Fig. 1a reveals that the NBs have a rectangular cross-section with widths of 400-500 nm and an average thickness of 50 nm. The XRD pattern (Fig. 1b) acquired from the NBs can be indexed to α-MoO_3 (JCPDS Card No. 05-0508), suggesting that the hydrothermal product is α-MoO_3 NBs. The HR-TEM image (ESI, Fig. S1†) and corresponding selected-area electron diffraction (SAED) pattern reveal that the as-produced α-MoO_3 NBs are single crystal. The lattice fringe spacings of about 0.184 nm and 0.198 nm correspond to the (002) and (200) planes of orthorombic α-MoO_3, respectively.

Fig. 2a displays the top-view SEM image of the free-standing MoO_3/GO multilayered film with 80 wt % MoO_3 NBs. The GO nanosheets that are uniformly distributed on the surface of MoO_3 NBs can be clearly indentified. The cross-sectional SEM image (Fig. 2b) discloses that the free-standing MoO_3/GO film has a thickness of about 12 μm. The digital image (inset in Fig. 2b) demonstrates good flexibility and mechanical integrity of the free-standing MoO_3/GO hybrid film although it does not contain any binders. The magnified cross-sectional SEM image in Fig. 2c clearly indicates that the free-standing MoO_3/GO film is composed of alternating stacked MoO_3 NBs and GO nanosheets. After nitridation in ammonia (NH_3) at 750 °C for 30 min, the overall shape of the film does not change obviously, however, the nanobelts become mesoporous (Fig. 2d and Fig. S2† (ESI)) and the GO nanosheets were reduced to rGO, as Raman Spectrum suggested (ESI, Fig. S3†). The XRD pattern of the nitrided composite film is a superposition of diffraction peaks from Mo_2N and rGO (ESI, Fig.S4†), further confirming that MoO_3/GO is converted into Mo_2N/rGO. The free-standing MMNNBs/rGO hybrid film is still very flexible and mechanically sturdy (inset in Fig. 2e) although it becomes slightly thinner (about 10 μm thickness) in comparison with the pristine MoO_3/GO multilayered film (about 12 μm) due to the reduction of GO, as indicated by Fig. 2e. The enlarged cross-section SEM image (Fig. 2f) reveals that the free-standing MMNNBs/rGO film is composed of alternating stacked Mo_2N NBs and rGO nanosheets.

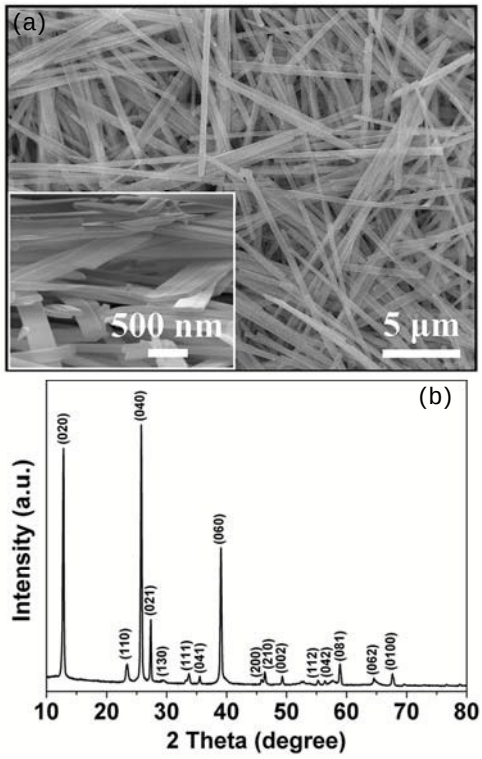

Fig. 1 (a) SEM image of MoO_3 nanobelts. Inset: the magnified SEM image of the nanobelts. (b) XRD patterns of MoO_3 nanobelts.

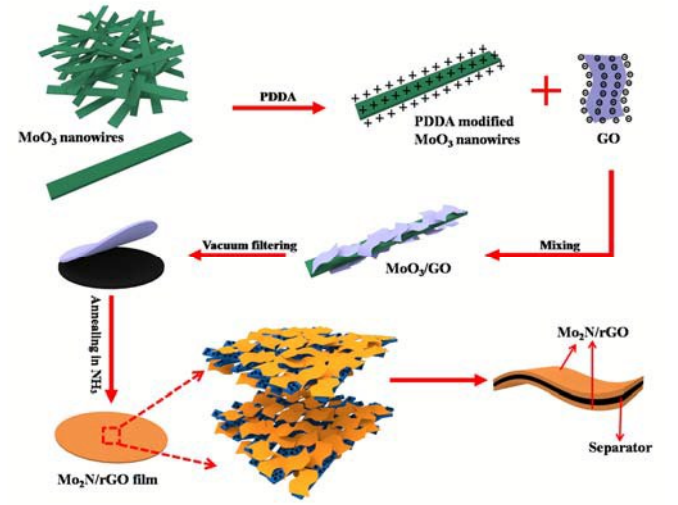

Scheme 1 Schematic fabrication procedures of flexible MMNNBs/rGO multilayed paper electrodes and flexible all-solid-state SCs.

The microstructure and composition of the MMNNBs/rGO multilayered hybrid films are further characterized by TEM, HR-TEM, and XPS. Fig. 3a indicates that the Mo_2N NBs and rGO (labeled with red word) strongly bond together even after ultrasonication in ethanol for 20 minutes prior to TEM characterization. The HR-TEM image in Fig. 3b clearly depicts the mesoporous morphology of Mo_2N nanobelts with a pore size of 3-8 nm. The mesoporous Mo_2N nanobelts provide a large surface area (ESI, Fig. S5†), thereby leading to better utilization of the pseudocapacitance of Mo_2N. The SAED pattern (insets in Fig. 3b) and HR-TEM image of the Mo_2N NBs (Fig. 3c) suggest that the Mo_2N nanobelt is single-crystal. The lattice fringe spacing is 0.21 nm which is consistent with the d-spacing of the (200) plane of cubic Mo_2N. Energy dispersive X-ray spectroscopy (EDS) demonstrates

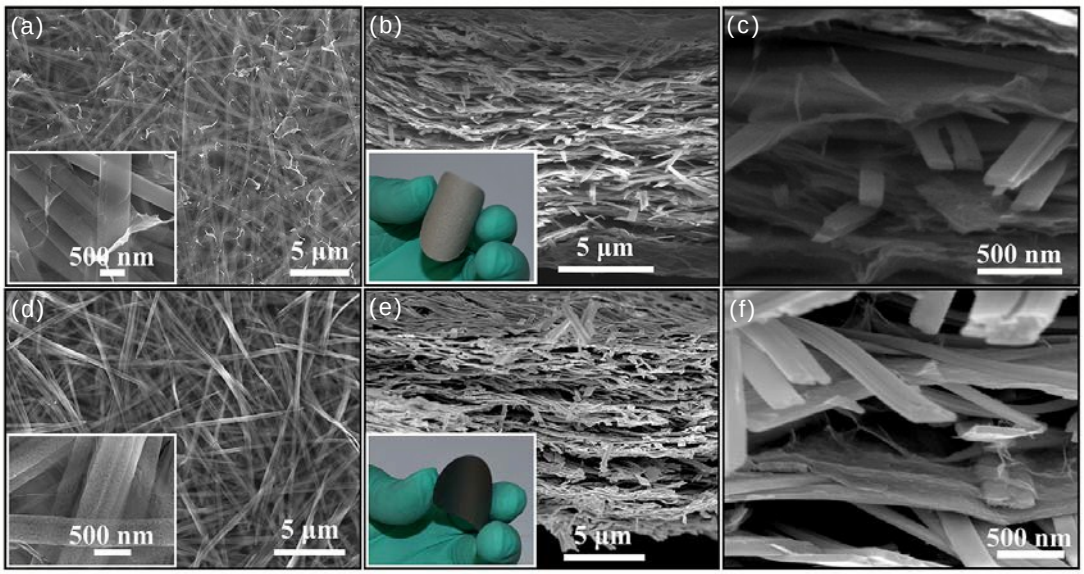

Fig. 2 (a) top-view SEM image of MoO_3/GO. Inset: magnified SEM image of the MoO_3/GO. Cross-section (b) and the enlarged cross-section (c) SEM images of the paper-like free-standing MoO_3/GO multilayered film. The inset in (b) is the digital image of the film electrode, demonstrating excellent flexibility. (d) top-view SEM image of MMNNBs/rGO. Inset: magnified SEM image of the MMNNBs/rGO. Cross-section (e) and the enlarged cross-section (f) SEM images of the paper-like free-standing MMNNBs/rGO hybrid electrode, showing the alternately stacked nanoarchitecture. The inset in (e) depicts the digital image of the paper-like free-standing MMNNBs/rGO hybrid electrode, demonstrating robust flexibility.

the presence of Mo, N, O, C, and Cu, corroborating that the hybrid film consists of rGO and Mo_2N (Fig. 3d). The Cu signal arises from the TEM grid and the O signal can be attributed to surface oxidation of Mo_2N and it can be further confirmed by XPS. The high-resolution XPS spectra of Mo 3d acquired from the MMNNBs/rGO hybride films reveal three different Mo states (ESI, Fig. S6†), including Mo_2N, molybdenum oxynitride, and molybdenum oxide. The high-resolution XPS spectra of Mo 3d acquired from the Mo_2N NBs powders prepared under the same experimental conditions show nearly the same Mo states, suggesting that the GO nanosheets have no effects on the conversion of MoO_3 into Mo_2N by thermal nitridation. The adsorption-desorption isotherm of the Mo_2N nanobelts discloses mesoporous characteristics. The BET specific surface area of the MMNNBs/rGO is smaller than those of Mo_2N and rGO, respectively, further implying the strong interaction between rGO nanosheets and Mo_2N nanobelts due to the formation of the stacked multilayered nanostructures (ESI, Fig. S5†). The thermogravimetry (TG) curves of the MMNNBs/rGO mulitilayered films show that the mass loading of MMNNBs is as high as 95.6 wt.% and rGO only accounts for about 4.4 wt.% in the free-standing MMNNBs/rGO multilayered film (ESI, Fig. S7†). Compared to the direct mixture of MMNNBs and rGO to form the free-standing film, the stacked MMNNBs/rGO multilayered film not only improves the loading mass of Mo_2N active materials (as high as 95.6 wt%) and mechanical flexibility of the electrode, but also facilitates rapid ion diffusion and electron transfer. Hence, large volumetric power and energy density associated with MMNNBs/rGO multilayered film are expected.

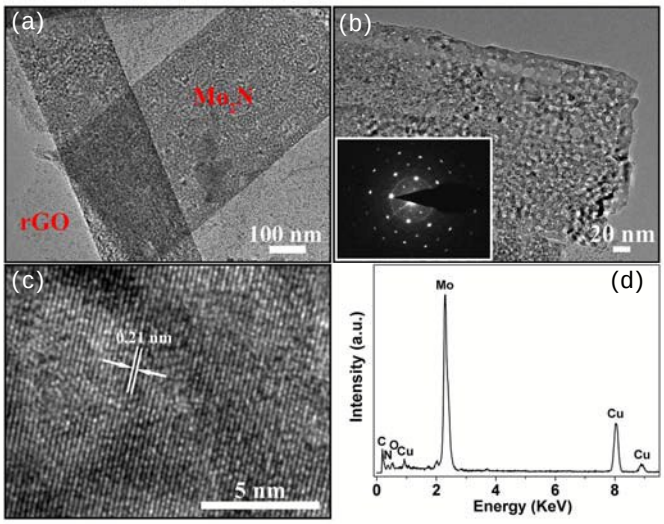

Fig. 3 (a, b) TEM images of paper-like free-standing MMNNBs/rGO hybrid electrode. The inset in (b) is SAED pattern. (c, d) Typical high-resolution TEM image of Mo_2N nanobelts and EDAX spectrum of free-standing MMNNBs/rGO multilayered film.

We first compare the capacitive performance of rGO, MMNNBs, and MMNNBs/rGO (95.6 wt.% Mo_2N) using a three-electrode system in a 1 M H_2SO_4 aqueous electrolyte at a scanning rate of 50 mV s^{-1} with a carbon plate as the counter electrode and a Ag/AgCl electrode as the reference electrode. Since MMNNBs cannot form a free-standing film by themselves, the capacitance measurements are carried out by mixing the electrode materials with 5 wt% acetylene black and a 5 wt% polytetrafluoroethylene (PTFE) suspension followed by pressing into a thin film using a double roller machine. The CV curves in Fig. 4a indicate that the capacitance of the MMNNBs electrode is larger than that of the rGO electrode under the same mass loading. In addition, four couples of redox peaks (-0.19/-0.13, -0.07/-0.04, 0.14/0.09 and 0.33/0.38 V) could be observed, representing the typical behavior of pseudocapacity. We have also performed the CV tests for MoO_3 and Mo_2N in the 1M H_2SO_4 aqueous electrolyte at the scan rate of 100 mV/s (ESI, Fig.

S8†). The two redox pairs at -0.07/-0.04 and 0.14/0.09 V could be observed both from CV curves of MoO_3 and Mo_2N. Thus, it could be safely concluded that two redox pairs at -0.07/-0.04 and 0.14/0.09 V are ascribed to redox reaction of surface oxidative layers on Mo_2N surface. The other two redox peaks at -0.19/-0.13 and 0.33/0.38 V should be from the redox reaction of Mo_2N in H_2SO_4 electrolyte.[36] The possible redox peaks can be attributed to the following reactions:[35]

$$Mo_2N+xH^++xe^- \leftrightarrow Mo_2N(H_{abs})_x \quad (1)$$

$$MoO_3+xH++xe- \leftrightarrow MoO_{3-x}(OH)_x \quad (2)$$

Although the MMNNBs/rGO composite contains 4.4 wt% rGO, the capacitance of the MMNNBs/rGO electrode is slightly larger than that of the MMNNBs electrode under the same conditions. The enhanced capacitance achieved from the MMNNBs/rGO electrode can be attributed to the synergistic effects of the good capacitive performance of MMNNBs and high conductivity of rGO.

Fig. 4b shows the CV curves of the flexible MMNNBs/rGO multilayered film electrodes at scanning rates between 50 and 1000 mV s^{-1} under a stable operation window between -0.25 and 0.45 V. All the CV curves exhibit a nearly ideal rectangular shape even at a large scanning rate of 1000 mV s^{-1} indicative of the superior capacitive behavior and high rate capability. The GCD curves at different current densities are shown in Fig. 4c and the capacitance of the electrode can be calculated by the following equations:

$$C=I\Delta t/\Delta E \quad (2)$$

$$C_s=C/S=I\Delta t/S\Delta E \quad (3)$$

where C is the total capacitance, C_s is the areal capacitance, I is the discharge current, Δt is the discharge time, ΔE is the potential window during the discharging process after the IR drop, and S is the effective electrode area. Fig. 4d shows the calculated areal capacitances of the MMNNBs/rGO multilayered film electrodes as a function of the current density. The MMNNBs/rGO hybrid electrode shows a high areal capacitance of 142 mF cm^{-2} at a current density of 1 mA cm^{-2}. Moreover, 69% of the initial capacitance is retained when the current density is increased 150 folds from 1 to 150 mA cm^{-2}. The areal capacitance of the MMNNBs/rGO multilayered film electrode is larger than those of hydrogenated ZnO core-shell nanocable electrodes (138.7 mF cm^{-2} at 1 mA cm^{-2}),[39] carbon-based electrodes (0.2-90 mF cm^{-2}),[46-48] and carbon nanoparticles/MnO_2 nanorods electrodes (109 mF cm^{-2} at 1 mA cm^{-2}),[49] and close to that of the free-standing mesoporous VN/CNT hybrid electrode (178 mF cm^{-2} at 1.1 mA cm^{-2}).[31] Moreover, the free-standing MMNNBs/rGO hybrid electrodes exhibit excellent long-term cycle life with 93% capacitance retention after 10,000 cycles (ESI, Fig. S9†) in aqueous SCs, suggesting excellent stability and durability. The corresponding gravimetric capacitance of the hybrid film at different current densities is provided in Fig. S10. (ESI) and we also compare the gravimetric capacitance of carbon, metal carbide and nitride active materials. (Table S1†, ESI)

The free-standing MMNNBs/rGO multilayered film electrode has good flexibility and electrochemical properties such as large specific capacitance, high rate capability, and long cycling stability and thus

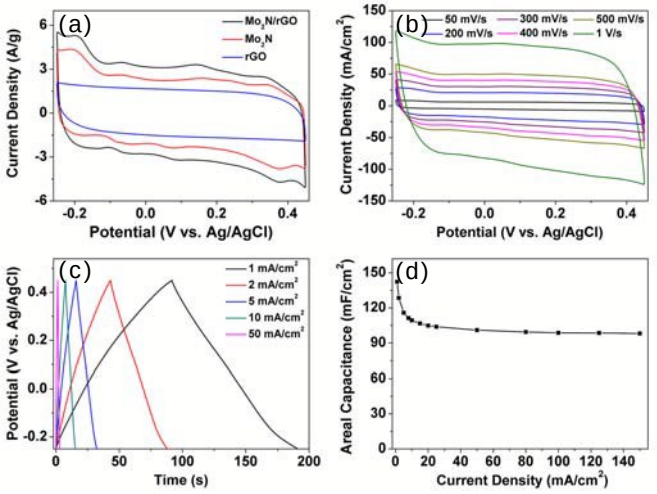

Fig. 4 (a) CV curves for rGO, Mo_2N and MMNNBs/rGO (4.38 wt% rGO) electrodes under the same mass loading at a san rate of 50 mV s^{-1}. (b) CV curves of frees-tanding MMNNBs/rGO film electrode (4.38 wt% rGO) at different scan rates ranging from 50 mV s^{-1} to 1 V s^{-1} in a 1 M H_2SO_4 aqueous electrolyte between -0.25 V and 0.45 V. (c) Galvanostatic charge-discharge curves of free-standing MMNNBs/rGO film electrode at a current density ranging from 1 mA cm^{-2} to 50 mA cm^{-2} between -0.25 V and 0.45 V. (d) Areal capacitance of free-standing MMNNBs/rGO film electrode as a function of the current density.

is a promising candidate for high-performance flexible SCs. To demonstrate the practicality, a flexible all-solid-state SC composed of two symmetrical freestanding MMNNBs/rGO multilayered film electrodes and the SiWA–H_3PO_4–PVA gel electrolyte is fabricated as illustrated in Scheme 1. Fig. 5a shows the CV curves of the assessed MMNNBs/rGO // MMNNBs/rGO symmetrical device in the voltage range of 0-0.7 V at scanning rates betweem 10 and 200 mV s^{-1}. The CV curves show a nearly rectangular mirror image with respect to the zero-current line, indicating the superior capacitive behavior. The volume of the cell is about 0.0035 cm^3 (1.4 cm × 0.5 cm × 0.005 cm), including the electrodes, electrolyte, and separator. The GCD curves obtained at various current densities are shown in Fig. 5b. The volumetric capacitances based on the whole device are calculated to be 15.4 and 9.8 F cm^{-3} at current densities of 100 and 1000 mA cm^{-3}, respectively (Fig. 5c). These values are substantially larger than those obtained from previously reported solid-state SCs such as free-standing mesoporous VN/CNT hybrid electrode based SCs (4 F cm^{-3} at 500 mA cm^{-3}),[31] hydrogenated ZnO MnO_2//Fe_2O_3 asymmetrical SCs (1.21 F cm^{-3} at 6.3 mA cm^{-3}),[44] graphene based SCs (0.45 F cm^{-3} at 4.5 mA cm^{-3})[50] and polypyrrole-coated paper based SCs (11 F cm^{-3} at 26.3 mA cm^{-3}).[51] Moreover, the all-solid-state SC device has superior rate capability with 64 % capacity retention when the current density is increased 10 times from 100 to 1000 mA cm^{-3}. The electrochemical impedance spectroscopy (EIS) data acquired from the all-solid-state flexible SC are displayed in Fig. 5d. The Nyquist plot exhibits a nearly vertical line along the imaginary axis in the low frequency region and the equivalent series resistance (ESR) of the device is about 7.6 Ω cm^2 (inset in Fig. 5d), indicating an excellent capacitive behavior.

The volumetric energy (E) and power (P) densities play key roles in the practical application of SCs and can be calculated as follows:

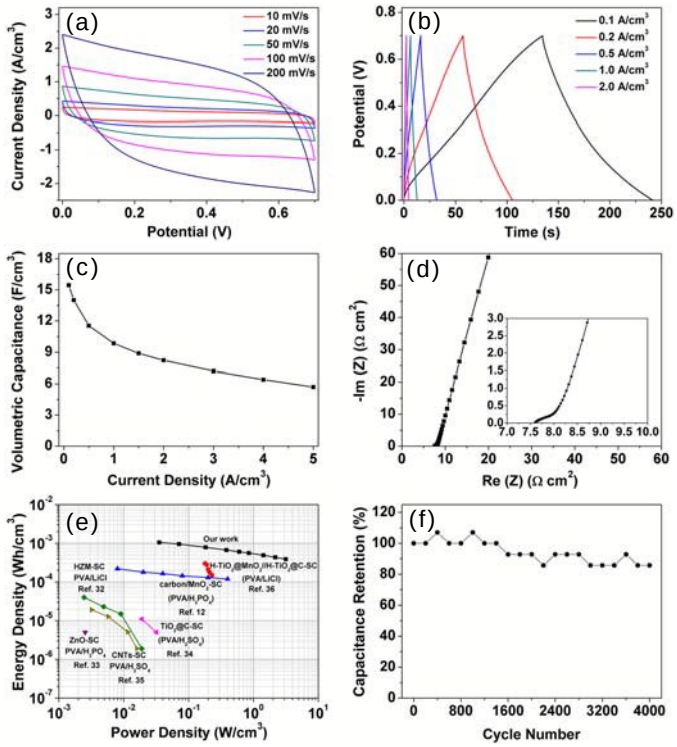

Fig. 5 Electrochemical performances of all-solid-state supercapacitor device based on MMNNBs/rGO hybrid electrodes and SiWA-H_3PO_4-PVA gel electrolyte. (a) CV curves. (b) Galvanostatic charge-discharge curves. (c) Volumetric capacitance as a function of current density. (d) Nyquist plots. (e) Ragone plot. (f) Cycle life. The energy and power densities reported for other SC devices are plotted in (e) for comparison.

$$E=CU^2/2V \quad (4)$$

$$P=E/t \quad (5)$$

where C is the total capacitance of the solid-state device, U is the operating voltage, V is the device volume, and t is the discharging time. The Ragone plots depicting the energy-power characteristics of our MMNNBs/rGO // MMNNBs/rGO symmetric devices and some of the reported all-solid-state SCs are summarized in Fig. 5e. An energy density of 1.05 mWh cm^{-3} can be achieved at a power density of 0.035 W cm^{-3} from the flexible MMNNBs/rGO // MMNNBs/rGO SCs and it remains at 0.39 mWh cm^{-3} at a power density of 3.15 W cm^{-3}. The volumetric energy density (1.05 mWh cm^{-3}) reported here is much larger than those reported previously from quasi and all-solid-state SCs such as carbon/MnO_2 core-shell fiber based SCs (0.22 mWh cm^{-3}, PVA/H_3PO_4),[38] hydrogenated single-crystal ZnO@amorphous ZnO-doped MnO_2 core-shell nanocable (HZM) based SCs (0.04 mWh cm^{-3}, PVA/LiCl),[39] ZnO nanowires based SCs (0.005 mWh cm^{-3}, PVA/H_3PO_4),[40] TiO_2@C core-shell nanowires based SCs (0.011 mWh cm^{-3}, PVA/H_2SO_4),[41] carbon nanotubes based SCs (0.02 mWh cm^{-3}, PVA/H_2SO_4),[42] and H-TiO_2@MnO_2//H-TiO_2@C core-shell based SCs (0.3 mWh cm^{-3}, PVA/LiCl).[45] The excellent electrochemical performance of the all-solid-state device can be attributed to the excellent capacitive properties of the freestanding MMNNBs/rGO multilayered film electrodes and high proton-conducting of SiWA–H_3PO_4–PVA) gel electrolyte, which provide not only high ionic conductivity, but also protons for the Faradaic redox reacions associated with Mo_2N.[52]

The long-term cycling stability, leakage currents, and self-discharging characteristics are important to practical applications of flexible SCs. Fig. 5f shows that the volumetric capacitance is 85.7 % of the initial capacitance after 4,000 charging-discharging cycles at a current density of 0.57 A cm^{-3}. Moreover, the SC has a small leakage current of about 20 μA (ESI, Fig. S11a†). The self-discharging test performed on the flexible MMNNBs/rGO //MMNNBs/rGO symmetrical SC reveals rapid self-discharging in the few minutes and finally an open-circuit voltage of 0.12 V beyond 24 h (ESI, Fig. S11b†), implying relatively high stability.

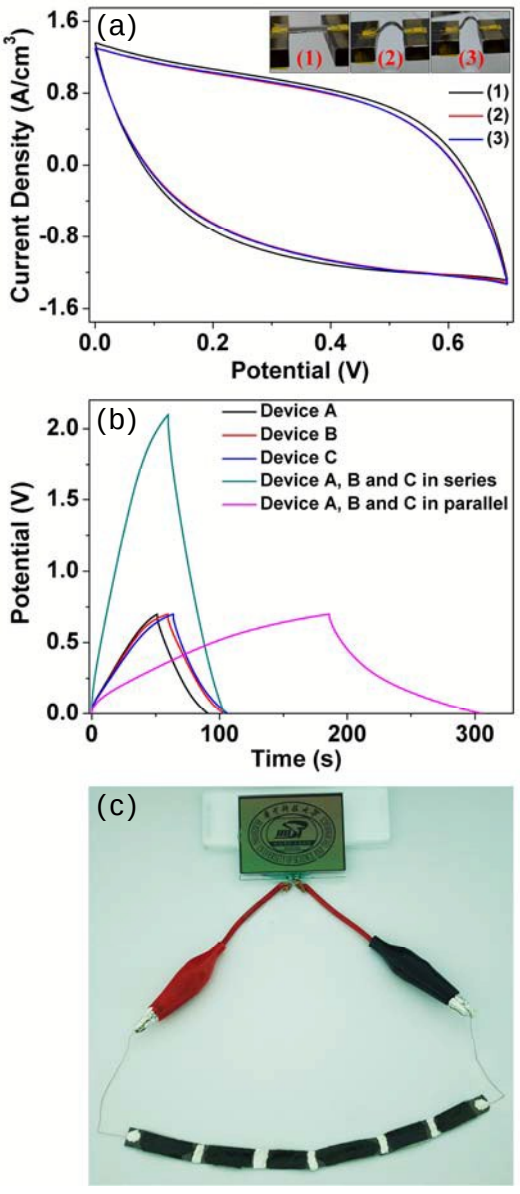

Fig. 6 (a) CV curves collected from an all-solid-state supercapacitor device at a scan rate of 100 mV s^{-1} under different bending states. Insets are the pictures under test conditions. (b) Galvanostatic charge-discharge curves for the as-fabricated all-solid-state SCs with different device configurations at a fixed current of 0.7 mA. (c) An application demo showing a liquid crystal display with a threshold voltage of 3 V could be powered by six devices in series.

In order to evaluate the practical feasibility of our device as a flexible energy storage component in flexible/wearable electronics, CV tests are conducted under different bending conditions. The CV curves under different bending conditions show no obvious change as shown in Fig. 6a. To further demonstrate the feasibility, three identical all-solid-state SCs are connected in series or parallel to construct the devices. The three units with a similar size of 1.4 cm × 0.5 cm × 0.005 cm are denoted as A, B, and C, respectively. The GCD curves of A, B, and C and the combinations in parallel and series acquired at the same current of 0.7 mA are shown in Fig. 6b. The capacitances of A, B, and C are 41.7, 46.3, and 44.1 mF, respectively. The charging/discharging voltage window of the three devices assembled in series shows 2.1 V with the same discharging time as a single one. The discharging time of the three devices in parallel is about 3 times longer than that of a single device and the capacitance of the three devices in parallel is 122.5 mF which is close to the theoretical value of 132.1 mF, thereby conforming to the basic rule of series and parallel assembly of capacitors. As a demonstrative usage of the highly flexible solid-state symmetric SCs, six SCs in series (each with size of ~ 0.7 cm × 1 cm × 0.005 cm) after being fully charged are used to drive a liquid crystal display (LCD) with a threshold voltage of 3 V. As shown in Fig. 6c, the LCD is lighted powerfully, demonstrating their promising applications in wearable or portable devices.

Conclusions

In summary, a facile and effective method to fabricate free-standing multilayered film electrodes consisting of alternating stacked mesoporous Mo_2N NBs and rGO nanosheets is described. In this architecture, the mesoporous Mo_2N NBs provide a large surface area and abundant active sites for charge storage and the rGO nanosheets between the Mo_2N NBs layers provide robust mechanical and flexible support. Hence, excellent capacitive properties, robust flexibility and mechanical integrity are accomplished. Compared to conventional free-standing film of the physical mixture of CNT or RGO and active materials, the stacked architecture not only obviously increases the mass loading of Mo_2N active materials (as large as 95.6 wt.%) while keeping the good mechanical integrity and flexibility, but also gives rise to high ion diffusion and electron transfer, resulting in large capacity and high rate capability simultaneously. The flexible MMNNBs/rGO multilayered film electrodes deliver large areal capacitances of 142 and 98 mF cm^{-2} at current densities of 1 and 150 mA cm^{-2} and excellent cycle stability with 93% of the initial capacitance retained after 10,000 cycles. The all-solid-state flexible SCs constructed by sandwiching two free-standing MMNNBs/rGO multilayered film electrodes with the SiWA–H_3PO_4–PVA gel electrolyte have a large volumetric capacitance of 15.4 F cm^{-3} and volume energy of 1.05 mWh cm^{-3} at a power density of 0.035 W cm^{-3}. After 4,000 charging-discharging cycles, 85.7% of the initial capacitance is retained, suggesting excellent cycle stability. Being flexible, environmentally friendly, and easily connected in series and parallel, the all-solid-state SCs have promising potentials in portable/wearable electronics.

Acknowledgements

G. Q. Ma and Z. Wang contributed equally to this work. This work was financially supported by the National Natural Science Foundation of China (51322210, 61434001), Fundamental Research Funds for the Central Universities (HUST: 0118187099), Director Fund of WNLO, City University of Hong Kong Strategic Research Grant (SRG) No. 7004188, and City University of Hong Kong Applied Research Grant ARG No. 9667085. The authors thank Prof. Jian Chen and Mr. Li Gong from Sun Yat-sen University (SYSU) for XPS characterization and facility provided by the Nanodevices and Characterization Center of WNLO, HUST.

Author Contributions

K. H. conceived the idea and designed the experiments. Mo_2N NBs, flexible electrodes and all-solid-state SCs were prepared by G. M. and Z. W.; The XRD and Raman data were collected by B. G. and X. P.; The electrochemical experiments were performed by G. M., B . G. and T. D. with technical input and direction from L. Y.and J. Z.; TEM and HRTEM images by J. S. and B. H.; The BET data were collected by Q. Z.; The final manuscript was prepared by G. M., K. H., P. C and all the authors discussed the results.

Notes and references

1 V. L. Pushparaj, M. M. Shaijumon, A. Kumar, S. Murugesan, L. Ci, R. Vajtai, R. J. Linhardt, O. Nalamasu, P. M. Ajayan, *Proc. Natl. Acad. Sci. USA*, 2007, **104,** 13574.
2 K. Jost, G. Dion, Y. Gogotsi, *J. Mater. Chem. A*, 2014, **2**, 10776.
3 X. Wang, X. Lu, B. Liu, D. Chen, Y. Tong, G. Shen, *Adv. Mater.*, 2014, **26**, 4763.
4 L. Li, Z. Wu, S. Yuan, X. B. Zhang, *Energy Environ. Sci.*, 2014, **7**, 2101.
5 X. Lu, M. Yu, G. Wang, Y. Tong, Y. Li, *Energy Environ. Sci.*, 2014, **7**, 2160.
6 P. Yang, W. Mai, *Nano Energy*, 2014, **8**, 274.
7 L. Yuan, X. Xiao, T. Ding, J. Zhong, X. Zhang, Y. Shen, B. Hu, Y. Huang, J. Zhou, Z. L. Wang, *Angew. Chem. Int. Ed.*, 2012, **124**, 5018.
8 C. Liu, F. Li, L. -P. Ma, H. -M. Cheng, *Adv. Mater.*, 2010, **22**, E28.
9 M. Beidaghi, Y. Gogotsi, *Energy Environ. Sci.*, 2014, **7**, 867.
10 P. Simon, Y. Gogotsi, *Nat. Mater.*, 2008, **7**, 845.
11 P. Simon, Y. Gogotsi, B. Dunn, *Science Magazine*, 2014, **343**, 1210.
12 L. L. Zhang, X. S. Zhao, *Chem. Soc. Rev.*, 2009, **38**, 2520.
13 Y. Wang, Z. Shi, Y. Huang, Y. Ma, C. Wang, M. Chen, Y. Chen, *J. Phys. Chem. C*, 2009, **113**, 13103.
14 Y. Huang, J. Liang, Y. Chen, *Small*, 2012, **8**, 1805.
15 W.-Y. Tsai, R. Lin, S. Murali, L. L. Zhang, J. K. McDonough, R. S. Ruoff, P. -L. Taberna, Y. Gogotsi, P. Simon, *Nano Energy*, 2013, **2**, 403.
16 Y. Wang, Y. Xia, *Adv. Mater.*, 2013, **25**, 5336.
17 X. Lu, T. Zhai, X. Zhang, Y. Shen, L. Yuan, B. Hu, L. Gong, J. Chen, Y. Gao, J. Zhou, Y. Tong, Z. L. Wang, *Adv. Mater.*, 2012, **24**, 938.
18 J. Liu, Zhang, H. B. Wu, J. Lin, Z. Shen, X. W. Lou, *Energy Environ. Sci.*, 2014, **7**, 3709.
19 X. Wang, M. Li, Z. Chang, Y. Yang, Y. Wu, X. Liu, *ACS Appl. Mater. Interfaces*, 2015, **7**, 2280.
20 T. Zhai, X. Lu, Y. Ling, M. Yu, G. Wang, T. Liu, C. Liang, Y. Tong, Y. Li, *Adv. Mater.*, 2014, **26**, 5869.

21 Z. Yang, F. Xu, W. Zhang, Z. Mei, B. Pei, X. Zhu, *J. Power Sources*, 2014, **246**, 24.
22 Q. Wang, J. Yan, Z. Fan, T. Wei, M. Zhang, X. Jing, *J. Power Sources*, 2014, **247**, 197.
23 H. Tang, J. Wang, H. Yin, H. Zhao, D. Wang, Z. Tang, *Adv. Mater.*, 2015, **27**, 1117.
24 M. Zhi, C. Xiang, J. Li, M. Li, N. Wu, *Nanoscale*, 2013, **5**, 72.
25 V. Augustyn, P. Simon, B. Dunn, *Energy Environ. Sci.*, 2014, **7**, 1597.
26 G. Wang, L. Zhang, J. Zhang, *Chem. Soc. Rev.*, 2012, **41**, 797.
27 K. Wang, H. Wu, Y. Meng, Z. Wei, *Small*, 2014, **10**, 14.
28 P. Pande, P. G. Rasmussen, L. T. Thompson, *J. Power Sources*, 2012, **207**, 212.
29 H. Pang, S. J. Ee, Y. Dong, X. Dong, P. Chen, *ChemElectroChem*, 2014, **1**, 1027.
30 X. Lu, T. Liu, T. Zhai, G. Wang, M. Yu, S. Xie, Y. Ling, C. Liang, Y. Tong, Y. Li, *Adv. Energy Mater.*, 2014, **4**, 1300994.
31 X. Xiao, X. Peng, H. Jin, T. Li, C. Zhang, B. Gao, B. Hu, K. Huo, J. Zhou, *Adv. Mater.*, 2013, **25**, 5091.
32 M.-S. Balogun, W. Qiu, W. Wang, P. Fang, X. Lu, Y. Tong, *J. Mater. Chem. A*, 2015, **3**, 1364.
33 A. S. Aricò, P. Bruce, B. Scrosati, J. –M. Tarascon, W. V. Schalkwijk, *Nat. Mater.*, 2005, **4**, 366.
34 Y. Gogotsi, P. Simon, *Science Magazine*, 2011, **334**, 917.
35 T. -C. Liu, W. G. Pell, B. E. Conway, *J. Electrochem. Soc.*, 1998, **145**, 1882.
36 X. Li, Y. Xing, H. Wang, H. Wang, W. Wang, X. Chen, *Trans. Nonferrous Met. Soc. China*, 2009, **19**, 620.
37 K. -H. Lee, Y. -W. Lee, A. -R. Ko, G. Cao, K. -W. Park, *J. Am. Ceram. Soc.*, 2013, **96**, 37.
38 X. Xiao, T. Li, P. Yang, Y. Gao, H. Jin, W. Ni, W. Zhan, X. Zhang, Y. Cao, J. Zhong, L. Gong, W. C. Yen, W. Mai, J. Chen, K. Huo, Y. L. Chueh, Z. L. Wang, J. Zhou, *ACS Nano*, 2012, **6**, 9200.
39 P. Yang, X. Xiao, Y. Li, Y. Ding, P. Qiang, X. Tan, W. Mai, Z. Lin, W. Wu, T. Li, H. Jin, P. Liu, J. Zhou, C. P. Wong, Z. L. Wang, *ACS Nano*, 2013, **7**, 2617.
40 J. Bae, M. K. Song, Y. J. Park, J. M. Kim, M. Liu, Z. L. Wang, *Angew. Chem. Int. Ed.*, 2011, **50**, 1683.
41 H. Zheng, T. Zhai, M. Yu, S. Xie, C. Liang, W. Zhao, S. C. Wang, Z. Zhang, X. Lu, *J. Mater. Chem. C*, 2013, **1**, 225.
42 Y. J. Kang, H. Chung, C. -H. Han, W. Kim, *Nanotechnology*, 2012, **23**, 065401.
43 X. Xiao, T. Li, Z. Peng, H. Jin, Q. Zhong, Q. Hu, B. Yao, Q. Luo, C. Zhang, L. Gong, J. Chen, Y. Gogotsi, J. Zhou, *Nano Energy*, 2014, **6**, 1.
44 X. Lu, Y. Zeng, M. Yu, T. Zhai, C. Liang, S.Xie, M. –S. Balogun, Y. Tong, *Adv. Mater.*, 2014, **26**, 3148.
45 X. Lu, M. Yu, G. Wang, T. Zhai, S. Xie, Y. Ling, Y. Tong, Y. Li, *Adv. Mater.*, 2013, **25**, 267.
46 Z. Weng, Y. Su, D. W. Wang, F. Li, J. Du, H. -M. Cheng, *Adv. Energy Mater.*, 2011, **1**, 917.
47 D. Pech, M. Brunet, H. Durou, P. Huang, V. Mochalin, Y. Gogotsi, P. -L. Taberna, P. Simon, *Nat. Nanotechnol.*, 2010, **5**, 651.
48 W. Gao, N. Singh, L. Song, Z. Liu, A. L. M. Reddy, L. Ci, R. Vajtai, Q. Zhang, B. Wei, P. M. Ajayan, *Nat. Nanotechnol.*, 2011, **6**, 496.
49 L. Yuan, X. -H. Lu, X. Xiao, T. Zhai, J. Dai, F. Zhang, B. Hu, X. Wang, L. Gong, J. Chen, C. Hu, Y. Tong, J. Zhou, Z. L. Wang, *ACS Nano*, 2012, **6**, 656.
50 M. F. El-Kady, V. Strong, S. Dubin, R. B. Kaner, *Science*, 2012, **335**, 1326.
51 L. Yuan, B. Yao, B. Hu, K. Huo, W. Chen, J. Zhou, *Energy Environ. Sci.*, 2013, **6**, 470.
52 H. Gao, K. Lian, *RSC Adv.*, 2014, **4**, 33091.

Journal Name

ARTICLE

The table of contents entry

High-performance flexible all-solid-state devices based on alternating stacked mesoporous Mo_2N nanobelts and reduced graphene oxide multilayered paper electrodes were achieved.

Keywords: molybdenum nitride, reduced grapheme oxide, mesoporous, supercapacitors

Guoqiang Ma, Zhe Wang, Biao Gao, Tianpeng Ding, Xiang Peng, Qize Zhong, Jun Su, Bin Hu, Longyan Yuan, Paul K Chu, Jun Zhou and Kaifu Huo*

Multilayered Paper-Like Electrodes Composed of Alternating Stacked Mesoporous Mo_2N Nanobelts and Reduced Graphene Oxide for Flexible All-Solid-State Supercapacitors